Published in final edited form as:
Aerosol Sci Technol. 2015 January ; 49(1): 24–34. doi:10.1080/02786826.2014.991439.

An *In Situ* Method for Sizing Insoluble Residues in Precipitation and Other Aqueous Samples

Jessica L. Axson[1], **Jessie M. Creamean**[3], **Amy L. Bondy**[2], **Sonja S. Capracotta**[4], **Katy Y. Warner**[5], and **Andrew P. Ault**[1,2]

[1]Department of Environmental Health Sciences, University of Michigan, Ann Arbor, Michigan, USA

[2]Department of Chemistry, University of Michigan, Ann Arbor, Michigan, USA

[3]Cooperative Institute for Research in Environmental Sciences, University of Colorado, Boulder, Colorado, USA

[4]Malvern Instruments, Westborough, Massachusetts, USA

[5]Division of Resources Management and Science, Yosemite National Park, El Portal, California, USA

Abstract

Particles are frequently incorporated into clouds or precipitation, influencing climate by acting as cloud condensation or ice nuclei, taking up coatings during cloud processing, and removing species through wet deposition. Many of these particles, particularly ice nuclei, can remain suspended within cloud droplets/crystals as insoluble residues. While previous studies have measured the soluble or bulk mass of species within clouds and precipitation, no studies to date have determined the number concentration and size distribution of insoluble residues in precipitation or cloud water using in situ methods. Herein, for the first time we demonstrate that Nanoparticle Tracking Analysis (NTA) is a powerful in situ method for determining the total number concentration, number size distribution, and surface area distribution of insoluble residues in precipitation, both of rain and melted snow. The method uses 500 μL or less of liquid sample and does not require sample modification. Number concentrations for the insoluble residues in aqueous precipitation samples ranged from 2.0–3.0(±0.3)×10^8 particles cm^{-3}, while surface area ranged from 1.8(±0.7)–3.2(±1.0)×10^7 μm^2 cm^{-3}. Number size distributions peaked between 133–150 nm, with both single and multi-modal character, while surface area distributions peaked between 173–270 nm. Comparison with electron microscopy of particles up to 10 μm show that, by number, > 97% residues are <1 μm in diameter, the upper limit of the NTA. The range of concentration and distribution properties indicates that insoluble residue properties vary with ambient aerosol concentrations, cloud microphysics, and meteorological dynamics. NTA has great potential for studying the role that insoluble residues play in critical atmospheric processes.

Address correspondence to: Andrew P. Ault, University of Michigan, M6116 SPH II, 1415 Washington Heights, Ann Arbor, MI 48109-2029, USA. aulta@umich.edu.

Introduction

The interactions between particles and clouds, fogs, and precipitation impact nearly every aspect of atmospheric chemistry and climate, including: atmospheric composition (Ravishankara, 1997; Herckes et al., 2007), droplet nucleation (Andreae and Rosenfeld, 2008), ice crystal formation (DeMott et al., 2010), wet deposition (Croft et al., 2010; Steltzer et al., 2009), in-droplet oxidation (Boris et al., 2014; Brandt and Elding, 1998; Rao and Collett, 1998; Alexander et al., 2009), and cyclone invigoration (Rosenfeld et al., 2011; Jenkins et al., 2008). Critical research questions that have been explored for decades now involve how the particles that are taken up into cloud water, fog, or precipitation impact the composition (Gioda et al., 2013; Post et al., 1991; Straub et al., 2007; Watanabe et al., 2010), oxidative capacity (Deguillaume et al., 2004), pH (Budhavant et al., 2014; Gioda et al., 2013), and other cloud water properties (Lee et al., 2011). Many prior studies have primarily focused on the soluble components present in rainwater, particularly inorganic ions, to assess the sources (Gioda et al., 2013; Twohy et al., 2009; Demirak, 2007) and secondary species (i.e. nitrates and sulfates) present (Demirak, 2007). Some studies have found that metals from dissolving dust or anthropogenic particles can drive important oxidation reactions, such as S(IV) to S(VI) in sulfate (Alexander et al., 2009; Rao and Collett, 1998). Others determined that cloud processing can lead to the uptake of sulfate and other species on particles (Harris et al., 2014; Ueda et al., 2014; Eck et al., 2012). Dissolution of mineral dust, such as $CaCO_3$, can additionally serve to neutralize acidic droplets (Budhavant et al., 2014). Despite the extensive literature on cloud water, fog, and precipitation to date, relatively little is known about the insoluble or partially soluble residues of particles taken up into these aqueous environments.

Insoluble residues have already provided a great deal of insight into atmospheric processes including aerosol-cloud-precipitation interactions from aerosols acting as cloud condensation nuclei (CCN) and ice nuclei (IN), particularly during the CalWater campaign (Ault et al., 2011; Creamean et al., 2013; Holecek et al., 2007; Creamean et al., 2014). CalWater studies focused on how particles acting as IN or CCN can modify the resulting precipitation (Ault et al., 2011; Creamean et al., 2013). While CCN are often composed of soluble or partially soluble material, IN tend to be insoluble (DeMott et al., 2003a; Creamean et al., 2014). Several studies have focused more specifically on how dust and bioaerosols can serve as IN to form cloud ice crystals, which can then enhance precipitation in clouds containing supercooled droplets (Yuter and Houze, 2003; Creamean et al., 2013; Bergeron, 1935; DeMott et al., 2003b). Aerosols can also inhibit precipitation when present in high number concentrations by acting as CCN and creating large populations of small cloud droplets, which delay the conversion of cloud water into precipitation (Borys et al., 2000; Andreae and Rosenfeld, 2008). In both cases, inducing and inhibiting precipitation, it is important to understand which particles can most likely act as CCN and/or IN. Prior studies used nebulized, resuspended particles from liquid precipitation in order to gain insight into the chemical composition, but due to the complexity of the resuspension process and low resuspension efficiencies (Ohata et al., 2013; Schwarz et al., 2012), the quantification of insoluble residue number concentration and size distribution has not been

possible. This is critical as a recent study has shown that ice cloud processing can increase the ice nucleating ability of particles that were residues (Wagner et al., 2012).

Several studies have been performed to quantify insoluble particles in rain and snow samples with a specific focus on black carbon (BC) and mineral dust (Dong et al., 2014; Drab et al., 2002; Li and Osada, 2007; Ohata et al., 2011; Ohata et al., 2013; Schwarz et al., 2013; Torres et al., 2014; Zdanowicz et al., 1998; Hadley et al., 2010; Hadley and Kirchstetter, 2012). For BC size distribution measurements in precipitation, Single-Particle Soot Photometers (SP2) are often utilized (Ohata et al., 2011; Ohata et al., 2013; Schwarz et al., 2013; Torres et al., 2014). In this method, BC residues are resuspended via nebulization into the SP2, which then measures the mass-equivalent diameter of the BC and the volume equivalent diameter is subsequently determined. Others have used offline techniques including optical microscope imaging, scanning electron microscopy (SEM), and transmission electron microscopy (TEM) to reconstruct particle size distributions and characteristics from dried samples (Drab et al., 2002; Li and Osada, 2007). The main focus of these offline studies was on dust particles and were limited to particles >0.3 μm. Particle counters, which operate by electrochemical methods, have been used to determine dust particle size distributions >0.6 μm (Dong et al., 2014; Zdanowicz et al., 1998). For each of these techniques, samples were not examined in situ and methods were focused on specific particle compositions at larger sizes (>0.3 μm). This is particularly limiting as recent field and laboratory studies have shown that secondary organic aerosol (SOA) formation occurs within cloud water through cloud processing (Lee et al., 2012; Lee et al., 2011; Ervens et al., 2011; Lim et al., 2010; Altieri et al., 2006; Turpin and Lim, 2001; Blando and Turpin, 2000; Hawkins et al., 2014), and models predict higher concentrations of those low solubility organic species than Henry's law or multiphase modeling would predict (Tilgner et al., 2005). This may indicate that precipitation residues can consist of insoluble, phase separated SOA that BC and dust measurements alone will not identify (Wurzler et al., 2000; Croft et al., 2010).

We present a new technique for obtaining the number concentration and size distribution for all insoluble residues <1 μm in precipitation samples using Nanoparticle Tracking Analysis (NTA). NTA is a unique, in situ method for counting and sizing particles suspended in a liquid, and has typically been used for studies involving, but not limited to: engineered nanoparticles, industrial materials, extracellular vesicles, viruses, protein aggregates, and drug delivery nanoparticles (Filipe et al., 2010; Nassar et al., 2009; Herrington et al., 2010; Kramberger et al., 2012). Herein, NTA was utilized to analyze insoluble residue particles found in melted snow samples collected from Yosemite National Park in February of 2013 and rain samples collected in Ann Arbor, Michigan in June and July of 2014. To our knowledge, this is the first time NTA has been employed to determine the number concentration and size distribution of environmental particles found in precipitation as insoluble residues. In addition, the size distributions collected using NTA were compared to those collected from other analytical techniques including dynamic light scattering (DLS), which also measure particles in liquids, and TEM to measure dried precipitation residues. This study serves as a benchmark for the size classification of not only insoluble residues found in precipitation, but also for any environmental liquid samples. Overall, our results aim to improve our understanding of the number concentration and size distribution of

insoluble particles in precipitation, which is important for determining the population of particles that serve as cloud seeds, alter in-cloud reactions, emerge after cloud processing, and are scavenged and wet deposited by falling precipitation.

1. Materials and Methods

1.1. Precipitation Samples

Samples of fresh fallen snow were collected during winter storms at two different locations in Yosemite National Park during February of 2013, at Badger Pass (2,200 m AMSL; 37.67°N, 119.65°W) and at Tuolumne Meadows (2,600 m AMSL; 37.87°N, 119.36°W). Samples were collected in 5-gallon PTFE-lined bags, sealed with a PTFE clip after collection, then frozen and stored 14–15 months until analysis. Fresh rain samples were collected in Ann Arbor, Michigan outside of the University of Michigan School of Public Health Building II (930 m AMSL; 42.28°N, 83.73°W) on June 24, 2014 and July 8, 2014. Samples were collected in 0.5-L glass jars previously rinsed with methanol followed by 18 MΩ MilliQ water, and stored at 4°C approximately 8–22 days until analysis. Following sample collection, both rain samples were filtered using 2-μm glass syringe filters to remove any visible macroscopic debris most likely deposited from the wind during the storms and not in the rain itself. Prior to analysis, all precipitation samples were vortexed to thoroughly mix and redistribute residues that had settled during storage and preparation.

1.2. Nanoparticle Tracking Analysis

NTA counts and sizes nano-sized particles within a liquid suspension by illuminating them using a laser source and individually tracking the particle's Brownian motion to determine their hydrodynamic diameter (Kramberger et al., 2012; Malloy, 2011). This approach to particle sizing has been used in more than 900 publications on materials with a wide variety of refractive indices. The NanoSight™ LM10 (NanoSight Ltd., Amesbury, UK) used in our experiments was equipped with a 20x objective microscope and c-mount specially designed to hold the laser module (Figure 1a). The laser module had temperature-control capabilities and contained a 405 nm laser diode, which was directed into a small, 350-μL, sample chamber (Figure 1a). The light scatter from particles was captured via a high sensitivity sCMOS camera (Hamamatsu, Orca). Videos were collected and analyzed using the NTA 3.0 (Build 60) software. Brownian motion from each individual particle was tracked to obtain a mean squared displacement value and diffusion coefficient [1] (Figure 1b).

$$\frac{(\overline{x,y})^2}{4}=D_t \quad [1]$$

The diffusion coefficient was used in the Stokes' Einstein equation to calculate the spherical hydrodynamic diameter equivalent (D_h) for each individual particle [2]:

$$D_h=\frac{K_B T}{12\pi\eta D_t} \quad [2]$$

where D_t is the diffusion coefficient, K_B is Boltzmann's constant, T is temperature, and η is solvent viscosity. The individual particle measurements were then combined to create a high resolution size distribution (Figure 1c). All diameters referred to in this work are given in hydrodynamic diameter and are not yet converted into an aerodynamic diameter, which is commonly used in atmospheric studies. Future studies will aim to determine the conversion from the hydrodynamic diameter into a more useable aerodynamic diameter for atmospheric particles.

The working particle size range for the NanoSight™ is in the submicron range, from 10 nm up to 2 μm, dependent upon the refractive index of the material (Carr and Wright, 2013). From previous NTA measurements, particles > 40 nm are efficiently traced regardless of refractive index. In this study, we used a sample dependent upper limit of 1μm with a lower limit observed around ~ 40 nm to ensure accurate number concentrations. This lower limit may indicate that the refractive index of the material is low and smaller (<40 nm) particles may be present, but does not rule out that there are possibly no particles present in significant concentration below 40 nm.

For this study, the NanoSight™ LM10 instrument was used to measure the number concentration and number size distribution of insoluble residues present in the melted Yosemite snow and Ann Arbor rain samples (Figure 1). Surface area was calculated from the number size distribution assuming spherical particles. The NanoSight™ has a variety of laser choices (405 nm, 488 nm, 532 nm, and 638 nm) for particle analysis; however, we determined that the 405 nm laser module was optimal for the detection and analysis of insoluble residues and maximized our detection capability in the submicron size range of the system (Malloy and Carr, 2006; Carr and Wright, 2013). Prior to the injection of each sample, a 10-second video of 18 MΩ MilliQ water was acquired to check the cell cleanliness (visual check only, not enough particles for number concentration or size distribution data observed). In order to capture 11 × 30 second videos, a 500-μL aliquot of each aqueous precipitation sample was used; of which 350-μL was loaded into the LM10 cell using a 1-mL syringe. The liquid sample was advanced via the syringe between each video to ensure new particles were measured. Due to the sample polydispersity, a greater number of short (30 s) videos were collected, as opposed to fewer, longer videos used for monodisperse samples. Sample videos were batch processed after each experiment providing the distribution in terms of size versus number concentration (particles cm^{-3}) in a liquid volume for each sample. Herein, particles cm^{-3} refer to number concentration per volume of liquid. The number size distribution was then converted to a surface area distribution assuming spherical particles. Raw data for the average number concentration, number size distribution, and surface area distribution, given in 64 bins/decade, was obtained for the 11 videos for each precipitation sample. Analysis took approximately 30–45 minutes per sample and each sample had an average of 875 particles or greater tracked per video analyzed. Standard error was calculated through the NTA 3.0 software using the average of the 11 videos, additional potential sources of error for this application to environmental samples includes a range of refractive indices within the sample and the video analysis algorithm, but the large (~900) number of publications utilizing NTA on a wide range of samples provide confidence in the veracity of the method.

1.3. Dynamic Light Scattering

Dynamic light scattering was performed using a Zetasizer 3600 (Malvern, Inc.) on the Badger Pass and Tuolumne Meadows snow melt samples. Aliquots of 1-mL were placed in a polystyrene cuvette for analysis and 30 runs or greater were acquired. Due to the polydispersity of the samples and in order to improve data quality and reproducibility, larger particles were removed from the sample via a 0.45-μm glass syringe filter. Intensity distribution data, with approximately 16 bins/decade, was used to obtain the particle diameter for intersample comparison. Given the polydispersity of the sample and range of refractive indices present it was difficult to obtain convergence from the intensity-based DLS measurements.

1.4. Transmission Electron Microscopy

A 5-μL droplet of the Tuolumne Meadows snow melt sample was deposited onto a copper TEM grid (Ted Pella, Inc.) and dried prior to analysis. At the Electron Microbeam Analysis Laboratory (EMAL) located at the University of Michigan, Ann Arbor, a JEOL 3011 High Resolution Electron Microscope was used to collect images of the sample. The JEOL 3011 was run at less than 1.5×10^{-5} Pa and at 300 kV. Images were captured using an ORCA-ER CCD camera. ImageJ software was used to generate projected area diameter (D_{pa}) for insoluble residue size distributions from these images. Insoluble residues were chosen at random on the TEM grid and care was taken to avoid duplicative counting. Size distributions were created from the 595 residues collected in the Tuolumne Meadows snow melt sample and distributed into 16 bins/decade.

2. Results and Discussion

Suspended particulate number size and surface area distributions from NTA of Badger Pass and Tuolumne Meadows snow melt samples are shown in Figure 2. Badger Pass contained a lower total number concentration $2.7(\pm0.2)\times10^{8}$ particles cm^{-3} of insoluble residues when compared to the sample collected on the same day at the Tuolumne Meadows, a site higher in altitude and with less local anthropogenic influence, $3.0(\pm0.2)\times10^{8}$ particles cm^{-3}. Number size distributions were log-normally fit to identify modes present in each distribution and the results are presented in Table 1. The number size distributions for both Badger Pass and Tuolumne Meadows were multi-modal, with primary modes in a similar size range around 133–148 nm and secondary modes at larger sizes, ranging from 227–261 nm. Additionally, Tuolumne Meadows had a third mode that was higher in concentration than the larger diameter mode and was centered at 80 nm.

Assuming a uniform density and the surface area of a volume-equivalent sphere for particle diameter, the surface area of the insoluble residues in solution (i.e. the surface area of the solid-liquid interface, not the liquid-air interface of the droplet) were calculated from the number size distribution. While not a true measure of surface area (Guyon et al., 2001) since morphology is ignored, this approximate surface area can still provide valuable information regarding the insoluble residue distribution. This is supported by the fact that most particles at remote mountain sites in this size range are spherical, or nearly so, such as organic carbon (spherical) or biomass burning (Malm et al., 2005; Ault et al., 2011). The surface area

distribution for Badger Pass showed a primary mode at 270 nm and a secondary mode at 148 nm. Tuolumne Meadows surface area distribution consisted of a primary mode at 173 nm and a secondary mode centered at 461 nm. This sample likely had greater dust incorporated due to height of sample collection, which may explain the lower diameter mode. Total surface area for the two Yosemite sites ranged from $2.5(\pm0.8)\times10^7$ μm^2 cm^{-3} at Badger Pass to $2.9(\pm0.1)\times10^7$ μm^2 cm^{-3} at Tuolumne Meadows. Determining the available surface area of for insoluble residues in the aqueous solution of precipitation is important because it can provide insight into the particle surface area available for reactions to occur upon or for dissolution to proceed from. Insoluble residues become concentrated by droplet scavenging, and since the number concentration of particles is ~10^8 in solution, versus ~10^2 to 10^3 at remote sites or 10^5 in polluted urban areas, it is unsurprising that the surface area of the insoluble residues in solution is higher than for the particles in the surrounding air. As an example of quantifying this effect, typical ambient particle surface area concentration for a nearby remote site is 30–60 μm^2 cm^{-3} (Creamean et al., 2011) versus ~10^7 in precipitation, thus the surface area of insoluble residues in droplets have 10^6 more surface area than ambient particles at the same site. This internal surface area is important as it may play a critical role in SOA formation or ice activation from IN (DeMott et al., 2003a; DeMott et al., 2010; Wurzler et al., 2000; Ervens et al., 2011). For instance, with more surface area available there might be an increase in possible ice nucleation sites on the particles, and therefore, an increase in the immersion IN efficiency of certain particles. The NanoSight™ was able to quantify the number concentration and number size distribution of insoluble residues for the Yosemite snow melt samples, which were in turn used to calculate surface area distributions with in the NTA 3.0 software. The NanoSight™ was also able to determine differences between particle intensity distributions at the different collection sites. Future studies will add insoluble residue size and concentration data to studies correlating immersion IN potential with chemical composition (Creamean et al., 2014).

In addition to the snow melt samples, rain samples were collected to determine how NTA would respond to different forms of precipitation. Figure 3 shows the number and corresponding surface area distribution for the insoluble residues in Ann Arbor June and July rain samples. Unlike the snow melt samples, the rain sample number size distributions appeared to contain only one mode when log-normally fit, which contained primary modes at 150 nm for June and at 134 nm for July. Similarly, the surface area distributions were unimodal with June containing a primary mode at 228 nm and July with a primary mode at 210 nm. The total number concentration for June was at $3.0(\pm0.3)\times10^8$ particles cm^{-3}, whereas July total number concentration was lower, at $2.0(\pm0.3)\times10^8$ particles cm^{-3} (Figure 3c). Total surface area for June was at $3.2(\pm1.0)\times10^7$ μm^2 cm^{-3} and for July at $1.8(\pm0.7)\times10^7$ μm^2 cm^{-3}. To examine the size and surface area distributions more closely, the fraction of insoluble residues for larger (>300 nm) particles was determined. This size range cut was chosen based on the lower size limit of the most sensitive BC and dust measurements performed in the previously mentioned studies of residue size distributions in rain and snow. There was not a large difference in total number concentrations observed between Badger Pass and Tuolumne Meadows and the percent of particles >300 nm was small at 5.2% and 5.5%, respectively. In contrast, the rain samples collected during different storms showed different total number concentrations, with June having a greater total

number concentration than July. However, even with this difference the insoluble residues >300 nm still contributed little to the overall concentration, at 6.5% and 4.9%, respectively. For the surface area, insoluble residues >300 nm for Badger Pass, Tuolumne Meadows, Ann Arbor June, and Ann Arbor July showed a greater contribution to the total surface area at 22.6%, 35.5%, 25.8% and 23.7%, respectively.

To validate the use of NTA as a suitable tool for insoluble residue analysis, number size distributions from Badger Pass and Tuolumne Meadows acquired using NTA were compared to those collected using DLS (Figure 4). Unlike NTA, which used in situ melted snow samples, the DLS samples had to be filtered because the system was unable to acquire size distributions due to the extent of polydispersity in the unfiltered samples, indicating a limitation of the DLS instrument for this type of analysis. DLS measurements of snow melt samples provided the same primary mode in the number size distribution that was observed by NTA, roughly 130–150 nm. However, as expected, when comparing an intensity-based technique to a number based technique, DLS was unable to capture the breadth of the size distribution that NTA measured. This was clear from the polydispersity errors that were given for each sample collected, indicating that the polydispersity of the sample was disrupting the computations of the DLS algorithms. These polydispersity errors led to an artificial narrowing of the DLS distribution when compared with number based NTA and TEM measurements.

Melted snow samples that were deposited on the TEM grids and dried contained an array of particulate matter residues, creating difficulty in imaging and sizing the insoluble residues. Figure 5 shows a representative TEM number size distribution and images from the Tuolumne Meadows sample demonstrating the diversity of the size and shape of material that dried on the substrate. The resulting reconstructed TEM number size distribution showed that the primary size mode of the particles imaged was at very small particle sizes (<30 nm). However, for these small residues (<100 nm) it was not possible to distinguish effloresced soluble material from material that was insoluble in situ. Elemental analysis in this size range was not able to confidently determine what might have been present, for example, water insoluble and water soluble organic carbon, as both are present in the sample. Due to our inability to differentiate insoluble and soluble material in the TEM image, the TEM number size distribution for Tuolumne Meadows was approximately 80 nm smaller than that acquired using NTA and DLS. An additional challenge with using the TEM was that this technique was performed under vacuum, which can alter the size and morphology of residues that were insoluble in solution, and therefore may not be representative of the actual in situ insoluble residues or sizes. Alteration of the sample through dehydration, either under ambient conditions or under the high vacuum of the TEM, can alter the sample and efflorescence of soluble material which interfered with counting insoluble residues, were the primary contributors to the large difference between the primary mode of the NTA and TEM number size distributions. These results indicate that removing the insoluble residues from the liquid solution, i.e. ex situ analysis, can cause difficulty in determining size distributions for these particles. NTA was an optimal solution for size and concentration analysis because it did not require sample preparation, and particles were be tracked while still suspended in solution.

In previous work, insoluble precipitation residues were resuspended using a Collision atomizer, dried, and chemically analyzed using single-particle mass spectrometry (Ault et al., 2011; Creamean et al., 2014; Creamean et al., 2013). We attempted this resuspension method into traditional ambient particle sizers using a scanning mobility particle sizer (SMPS; measures 10–740 nm diameter particles) and aerosol particle sizer (APS; measures 0.54–19.8 μm diameter particles), which are typically used for ambient aerosol size distribution measurements. These results were unusable as the resuspended particles were overwhelmed by the formation of pure water droplets and particles from soluble species (distribution from 14–740 nm, mode at 350 nm), which was most likely due to the particle generation and drying technique. This is consistent with previous attempts to resuspend BC particles using a Collision atomizer that found very low Collision atomizer efficiencies when resuspending BC (Ohata et al., 2011; Ohata et al., 2013; Schwarz et al., 2013; Torres et al., 2014; Schwarz et al., 2012).

3. Conclusions

We have demonstrated a new method, NTA, for in situ analysis of insoluble particulate residues in rain and melted snow. NTA proved to be a powerful tool for the measurement of insoluble residues in snow and rain precipitation by distinguishing subtle differences in concentration and size distributions. Advantages of using NTA include: minimal sample preparation, small sample volume for analysis (<500 μL), high resolution submicron particle measurements down to 10 nm for metallic particles and 30 nm for polymeric-type particles, ease of operation, and speed of sample analysis.

NTA has great potential for improving our understanding of the role that insoluble residues play in critical atmospheric processes and can be applied to a wide range of atmospheric systems including fog water, rainwater, cloud water (liquid, mixed phase, and ice clouds), in-cloud surface sampling, surface snow deposition, ice cores, and cloud chamber studies. This technique can improve our understanding of how atmospheric particles that are taken up into cloud water, fog, or precipitation impact cloud composition and properties. Concentration and size distributions can be monitored as changes in cloud chemistry occur including change in pH, in-cloud oxidation, and uptake of insoluble organics. Insoluble residues from precipitation may be able to be distinguished from those dry deposited on snow pack surfaces by their sizes and concentrations. NTA has the potential to be a powerful tool in determining changes to insoluble residues as they undergo physical and chemical changes in atmospheric and climatologically important systems.

Acknowledgments

The authors would like to acknowledge Dean Martin Philbert of the School of Public Health at the University of Michigan and Professor Andrew Maynard of the Risk Science Center at Michigan for allowing us to use the NanoSight™ LM10 instrument. Dr. Pamela Wong of the Department of Biological Chemistry at the University of Michigan Medical School under Prof. Ari Gafini is acknowledged for the use of the DLS instrument. Daniel Gardner assisted with SMPS and APS measurements. The Electron Microbeam Analysis Laboratory (EMAL) at the University of Michigan is acknowledged for assistance with electron microscopy. We would like to acknowledge the Yosemite staff who helped with snow sample collection, particularly Rebecca Rising and Rob and Laura Pilewski. Desmond Madu and Jackelyn Rodriguez assisted with the rainwater collection and analysis. This project was supported through startup funds by the University of Michigan. J. Axson was funded by NIH Grant 5U01ES020128. J. Creamean was funded by the National Research Council Research Associate Program.

References

Alexander B, Park RJ, Jacob DJ, Gong SL. Transition metal-catalyzed oxidation of atmospheric sulfur: Global implications for the sulfur budget. J Geophys Res-Atmos. 2009; 114:1–13.10.1029/2008JD010486

Altieri KE, Carlton AG, Lim HJ, Turpin BJ, Seitzinger SP. Evidence for oligomer formation in clouds: Reactions of isoprene oxidation products. Environ Sci Technol. 2006; 40:4956–4960.10.1021/es052170n [PubMed: 16955892]

Andreae MO, Rosenfeld D. Aerosol-cloud-precipitation interactions. Part 1 The nature and sources of cloud-active aerosols. Earth-Sci Rev. 2008; 89:13–41.10.1016/j.earscirev.2008.03.001

Ault AP, Williams CR, White AB, Neiman PJ, Creamean JM, Gaston CJ, Ralph FM, Prather KA. Detection of Asian dust in California orographic precipitation. J Geophys Res-Atmos. 2011; 116:1–15.10.1029/2010JD015351

Bergeron, T. On the physics of cloud and precipitation. 5th Assembly of the U.G.G.I; Paul Dupont, Paris. 1935.

Blando JD, Turpin BJ. Secondary organic aerosol formation in cloud and fog droplets: a literature evaluation of plausibility. Atmos Environ. 2000; 34:1623–1632.10.1016/s1352-2310(99)00392-1

Boris AJ, Desyaterik Y, Collett JL. How do components of real cloud water affect aqueous pyruvate oxidation? Atmos Res. 2014; 143:95–106.10.1016/j.atmosres.2014.02.004

Borys RD, Lowenthal DH, Mitchell DL. The relationships among cloud microphysics, chemistry, and precipitation rate in cold mountain clouds. Atmos Environ. 2000; 34:2593–2602.10.1016/S1352-2310(99)00492-6

Brandt C, Elding LI. Role of chromium and vanadium in the atmospheric oxidation of sulfur (IV). Atmos Environ. 1998; 32:797–800.10.1016/S1352-2310(97)00331-2

Budhavant KB, Rao PSP, Safai PD, Granat L, Rodhe H. Chemical composition of the inorganic fraction of cloud-water at a high altitude station in West India. Atmos Environ. 2014; 88:59–65.10.1016/j.atmosenv.2014.01.039

Creamean JM, Ault AP, Ten Hoeve JE, Jacobson MZ, Roberts GC, Prather KA. Measurements of Aerosol Chemistry during New Particle Formation Events at a Remote Rural Mountain Site. Environ Sci Technol. 2011; 45:8208–8216.10.1021/es103692f [PubMed: 21809849]

Creamean JM, Suski KJ, Rosenfeld D, Cazorla A, DeMott PJ, Sullivan RC, White AB, Ralph FM, Minnis P, Comstock JM, Tomlinson JM, Prather KA. Dust and Biological Aerosols from the Sahara and Asia Influence Precipitation in the Western U.S. Science. 2013; 339:1572–1578.10.1126/science.1227279 [PubMed: 23449996]

Creamean JM, Lee C, Hill TC, Ault AP, DeMott PJ, White AB, Ralph FM, Prather KA. Chemical properties of insoluble precipitation residues. J Aerosol Sci. 2014; 76:13–27.

Croft B, Lohmann U, Martin RV, Stier P, Wurzler S, Feichter J, Hoose C, Heikkila U, van Donkelaar A, Ferrachat S. Influences of in-cloud aerosol scavenging parameterizations on aerosol concentrations and wet deposition in ECHAM5-HAM. Atmos Chem Phys. 2010; 10:1511–1543.

Deguillaume L, Leriche M, Monod A, Chaumerliac N. The role of transition metal ions on HOx radicals in clouds: a numerical evaluation of its impact on multiphase chemistry. Atmos Chem Phys. 2004; 4:95–110.10.5194/acp-4-95-2004

Demirak A. The Influence of a Coal-Fired Power Plant in Turkey on the Chemical Composition of Rain Water in a Certain Region. Environ Monit Assess. 2007; 129:189–196.10.1007/s10661-006-9352-0 [PubMed: 17057977]

DeMott PJ, Cziczo DJ, Prenni AJ, Murphy DM, Kreidenweis SM, Thomson DS, Borys R, Rogers DC. Measurements of the concentration and composition of nuclei for cirrus formation. P Natl Acad Sci USA. 2003a; 100:14655–14660.10.1073/pnas.2532677100

DeMott PJ, Sassen K, Poellot MR, Baumgardner D, Rogers DC, Brooks SD, Prenni AJ, Kreidenweis SM. African dust aerosols as atmospheric ice nuclei. Geophys Res Lett. 2003b: 30.10.1029/2003gl017410

DeMott PJ, Prenni AJ, Liu X, Kreidenweis SM, Petters MD, Twohy CH, Richardson MS, Eidhammer T, Rogers DC. Predicting global atmospheric ice nuclei distributions and their impacts on climate. P Natl Acad Sci USA. 2010; 107:11217–11222.10.1073/pnas.0910818107

Dong ZW, Qin DH, Kang SC, Ren JW, Chen JZ, Cui XQ, Du ZH, Qin X. Physicochemical characteristics and sources of atmospheric dust deposition in snow packs on the glaciers of western Qilian Mountains, China. Tellus Ser B-Chem Phys Meteorol. 2014; 66:1–15.10.3402/tellusb.v66.20956

Drab E, Gaudichet A, Jaffrezo JL, Colin JL. Mineral particles content in recent snow at Summit (Greenland). Atmos Environ. 2002; 36:5365–5376.10.1016/s1352-2310(02)00470-3

Eck TF, Holben BN, Reid JS, Giles DM, Rivas MA, Singh RP, Tripathi SN, Bruegge CJ, Platnick S, Arnold GT, Krotkov NA, Carn SA, Sinyuk A, Dubovik O, Arola A, Schafer JS, Artaxo P, Smirnov A, Chen H, Goloub P. Fog- and cloud-induced aerosol modification observed by the Aerosol Robotic Network (AERONET). J Geophys Res-Atmos. 2012; 11710.1029/2011jd016839

Ervens B, Turpin BJ, Weber RJ. Secondary organic aerosol formation in cloud droplets and aqueous particles (aqSOA): a review of laboratory, field and model studies. Atmos Chem Phys. 2011; 11:11069–11102.10.5194/acp-11-11069-2011

Filipe V, Hawe A, Jiskoot W. Critical Evaluation of Nanoparticle Tracking Analysis (NTA) by NanoSight for the Measurement of Nanoparticles and Protein Aggregates. Pharm Res-Dordr. 2010; 27:796–810.10.1007/s11095-010-0073-2

Gioda A, Mayol-Bracero OL, Scatena FN, Weathers KC, Mateus VL, McDowell WH. Chemical constituents in clouds and rainwater in the Puerto Rican rainforest: Potential sources and seasonal drivers. Atmos Environ. 2013; 68:208–220.10.1016/j.atmosenv.2012.11.017

Guyon, E.; Hulin, J.; Petit, L.; Mitescu, CD. Physical Hydrodynamics. 1. Oxford University Press; Oxford: 2001.

Hadley OL, Corrigan CE, Kirchstetter TW, Cliff SS, Ramanathan V. Measured black carbon deposition on the Sierra Nevada snow pack and implication for snow pack retreat. Atmos Chem Phys. 2010; 10:7505–7513.10.5194/acp-10-7505-2010

Hadley OL, Kirchstetter TW. Black-carbon reduction of snow albedo. Nat Clim Chang. 2012; 2:437–440.10.1038/nclimate1433

Harris E, Sinha B, van Pinxteren D, Schneider J, Poulain L, Collett J, D'Anna B, Fahlbusch B, Foley S, Fomba KW, George C, Gnauk T, Henning S, Lee T, Mertes S, Roth A, Stratmann F, Borrmann S, Hoppe P, Herrmann H. In-cloud sulfate addition to single particles resolved with sulfur isotope analysis during HCCT-2010. Atmos Chem Phys. 2014; 14:4219–4235.10.5194/acp-14-4219-2014

Hawkins LN, Baril MJ, Sedehi N, Galloway MM, De Haan DO, Schill GP, Tolbert MA. Formation of Semisolid, Oligomerized Aqueous SOA: Lab Simulations of Cloud Processing. Environ Sci Technol. 2014; 48:2273–2280.10.1021/es4049626 [PubMed: 24428707]

Herckes P, Chang H, Lee T, Collett J Jr. Air Pollution Processing by Radiation Fogs. Water Air Soil Pollut. 2007; 181:65–75.10.1007/s11270-006-9276-x

Herrington MR, Buchnev O, Kaczmarek M, Nandhakumar I. The Effect of the Size of BaTiO3 Nanoparticles on the Electro-Optic Properties of Nematic Liquid Crystals. Mol Cryst Liq Cryst. 2010; 527:72–79.10.1080/15421406.2010.486362

Holecek JC, Spencer MT, Prather KA. Analysis of rainwater samples: Comparison of single particle residues with ambient particle chemistry from the northeast Pacific and Indian oceans. J Geophys Res-Atmos. 2007; 112:1–10.10.1029/2006jd008269

Jenkins GS, Pratt AS, Heymsfield A. Possible linkages between Saharan dust and tropical cyclone rain band invigoration in the eastern Atlantic during NAMMA-06. Geophys Res Lett. 2008; 35:1–7.10.1029/2008gl034072

Kramberger P, Ciringer M, Strancar A, Peterka M. Evaluation of nanoparticle tracking analysis for total virus particle determination. Virol J. 2012; 9:1–10.10.1186/1743-422x-9-265 [PubMed: 22214262]

Lee AKY, Herckes P, Leaitch WR, Macdonald AM, Abbatt JPD. Aqueous OH oxidation of ambient organic aerosol and cloud water organics: Formation of highly oxidized products. Geophys Res Lett. 2011; 38:1–5.10.1029/2011gl047439

Lee AKY, Hayden KL, Herckes P, Leaitch WR, Liggio J, Macdonald AM, Abbatt JPD. Characterization of aerosol and cloud water at a mountain site during WACS 2010: secondary organic aerosol formation through oxidative cloud processing. Atmos Chem Phys. 2012; 12:7103–7116.10.5194/acp-12-7103-2012

Li JM, Osada K. Water-insoluble particles in spring snow at Mt. Tateyama, Japan: Characteristics of the shape factors and size distribution in relation with their origin and transportation. J Meteorol Soc Jpn. 2007; 85:137–149.10.2151/jmsj.85.137

Lim YB, Tan Y, Perri MJ, Seitzinger SP, Turpin BJ. Aqueous chemistry and its role in secondary organic aerosol (SOA) formation. Atmos Chem Phys. 2010; 10:10521–10539.10.5194/acp-10-10521-2010

Malloy A, Carr B. Nanoparticle tracking analysis - The Halo (TM) system. Particle & Particle Systems Characterization. 2006; 23:197–204.10.1002/ppsc.200601031

Malloy A. Count, size and visualize nanoparticles. Materials Today. 2011; 14:170–173.

Malm WC, Day DE, Carrico C, Kreidenweis SM, Collett JL, McMeeking G, Lee T, Carrillo J, Schichtel B. Intercomparison and closure calculations using measurements of aerosol species and optical properties during the Yosemite Aerosol Characterization Study. J Geophys Res-Atmos. 2005; 11010.1029/2004jd005494

Nassar T, Rom A, Nyska A, Benita S. Novel double coated nanocapsules for intestinal delivery and enhanced oral bioavailability of tacrolimus, a P-gp substrate drug. J Control Release. 2009; 133:77–84.10.1016/j.jconrel.2008.08.021 [PubMed: 18822327]

Ohata S, Moteki N, Kondo Y. Evaluation of a Method for Measurement of the Concentration and Size Distribution of Black Carbon Particles Suspended in Rainwater. Aerosol Science and Technology. 2011; 45:1326–1336.10.1080/02786826.2011.593590

Ohata S, Moteki N, Schwarz J, Fahey D, Kondo Y. Evaluation of a Method to Measure Black Carbon Particles Suspended in Rainwater and Snow Samples. Aerosol Science and Technology. 2013; 47:1073–1082.10.1080/02786826.2013.824067

Post D, Bridgman HA, Ayers GP. Fog and rainwater composition in rural SE Australia. J Atmos Chem. 1991; 13:83–95.10.1007/bf00048102

Rao X, Collett JL. The drop size-dependence of iron and manganese concentrations in clouds and fogs: Implications for sulfate production. J Atmos Chem. 1998; 30:273–289.10.1023/a:1006044614291

Ravishankara AR. Heterogeneous and multiphase chemistry in the troposphere. Science. 1997; 276:1058–1065.

Rosenfeld D, Clavner M, Nirel R. Pollution and dust aerosols modulating tropical cyclones intensities. Atmos Res. 2011; 102:66–76.10.1016/j.atmosres.2011.06.006

Schwarz JP, Doherty SJ, Li F, Ruggiero ST, Tanner CE, Perring AE, Gao RS, Fahey DW. Assessing Single Particle Soot Photometer and Integrating Sphere/Integrating Sandwich Spectrophotometer measurement techniques for quantifying black carbon concentration in snow. Atmos Meas Tech. 2012; 5:2581–2592.10.5194/amt-5-2581-2012

Schwarz JP, Gao RS, Perring AE, Spackman JR, Fahey DW. Black carbon aerosol size in snow. Sci Rep. 2013; 3:1–5.10.1038/srep01356

Steltzer H, Landry C, Painter TH, Anderson J, Ayres E. Biological consequences of earlier snowmelt from desert dust deposition in alpine landscapes. P Natl Acad Sci USA. 2009; 106:11629–11634.10.1073/pnas.0900758106

Straub DJ, Lee T, Collett JL. Chemical composition of marine stratocumulus clouds over the eastern Pacific Ocean. J Geophys Res-Atmos. 2007; 11210.1029/2006jd007439

Tilgner A, Majdik Z, Sehili AM, Simmel M, Wolke R, Herrmann H. SPACCIM: Simulations of the multiphase chemistry occurring in the FEBUKO hill cap cloud experiments. Atmos Environ. 2005; 39:4389–4401.10.1016/j.atmosenv.2005.02.028

Torres A, Bond TC, Lehmann CMB, Subramanian R, Hadley OL. Measuring Organic Carbon and Black Carbon in Rainwater: Evaluation of Methods. Aerosol Science and Technology. 2014; 48:239–250.10.1080/02786826.2013.868596

Turpin BJ, Lim HJ. Species contributions to PM2.5 mass concentrations: Revisiting common assumptions for estimating organic mass. Aerosol Science and Technology. 2001; 35:602–610.10.1080/02786820152051454

Twohy CH, Kreidenweis SM, Eidhammer T, Browell EV, Heymsfield AJ, Bansemer AR, Anderson BE, Chen G, Ismail S, DeMott PJ, Van den Heever SC. Saharan dust particles nucleate droplets in eastern Atlantic clouds. Geophys Res Lett. 2009; 36:1–6.

Ueda S, Hirose Y, Miura K, Okochi H. Individual aerosol particles in and below clouds along a Mt. Fuji slope: Modification of sea-salt-containing particles by in-cloud processing. Atmos Res. 2014; 137:216–227.10.1016/j.atmosres.2013.10.011

Wagner R, Mohler O, Saathoff H, Schnaiter M, Skrotzki J, Leisner T, Wilson TW, Malkin TL, Murray BJ. Ice cloud processing of ultra-viscous/glassy aerosol particles leads to enhanced ice nucleation ability. Atmos Chem Phys. 2012; 12:8589–8610.10.5194/acp-12-8589-2012

Watanabe K, Honoki H, Iwai A, Tomatsu A, Noritake K, Miyashita N, Yamada K, Yamada H, Kawamura H, Aoki K. Chemical Characteristics of Fog Water at Mt. Tateyama, Near the Coast of the Japan Sea in Central Japan. Water, Air, & Soil Pollution. 2010; 211:379–393.10.1007/s11270-009-0307-2

Wurzler S, Reisin TG, Levin Z. Modification of mineral dust particles by cloud processing and subsequent effects on drop size distributions. J Geophys Res-Atmos. 2000; 105:4501–4512.10.1029/1999jd900980

Yuter SE, Houze RA. Microphysical modes of precipitation growth determined by S-band vertically pointing radar in orographic precipitation during MAP. Q J Roy Meteor Soc. 2003; 129:455–476.10.1256/Qj.01.216

Zdanowicz CM, Zielinski GA, Wake CP. Characteristics of modern atmospheric dust deposition in snow on the Penny Ice Cap, Baffin Island, Arctic Canada. Tellus Ser B-Chem Phys Meteorol. 1998; 50:506–520.10.1034/j.1600-0889.1998.t01-1-00008.x

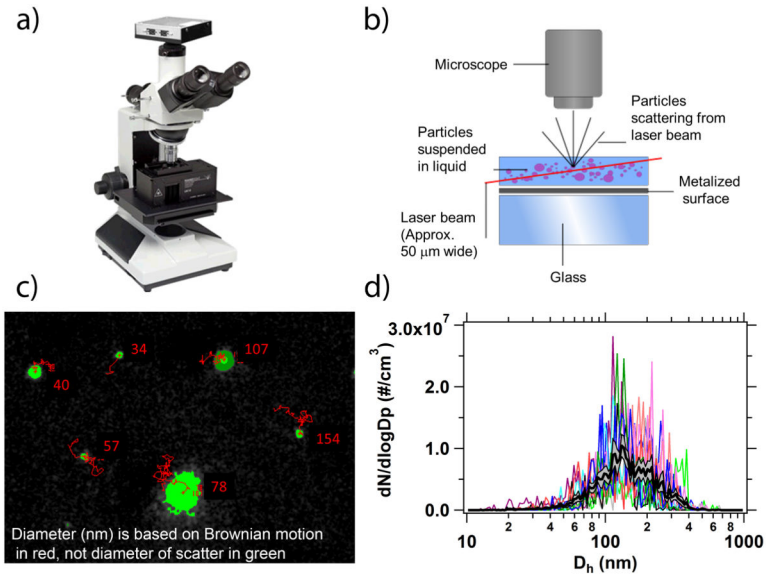

Figure 1.

a) An image of the NanoSight™ LM10 instrument used in this study and a b) schematic of the laser illumination device (schematic courtesy of Malvern, Inc.). c) The NTA 3.0 software tracked the Brownian motion (red lines) of individual nanoparticles (green spheres) to determine their D_h. Note that the diameter is based on Brownian motion and not the diameter of the scatter (green). d) Multiple size distributions for each sample were collected, with the average of those distributions shown in black with the (grey) shaded region indicating the ± 1 standard error of the mean.

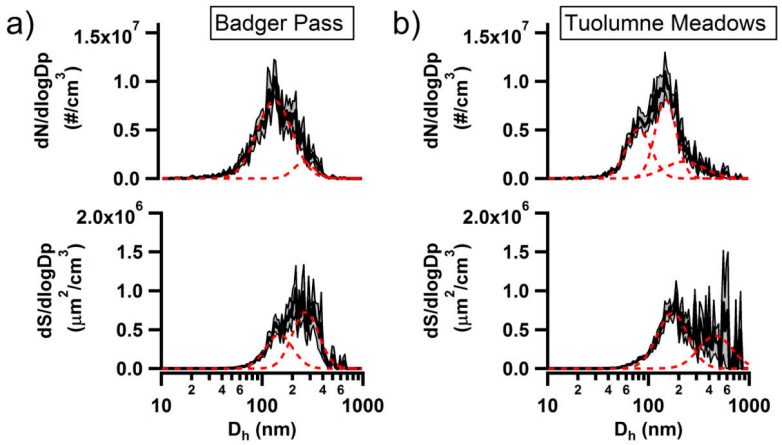

Figure 2.

Log-normal number size and surface area distributions collected using NTA for the a) Badger Pass and b) Tuolumne Meadows snow melt samples. The dashed (red) lines are log-normal fits for the number size and surface area distributions and the (grey) shaded regions indicate the ± 1 standard error of the mean.

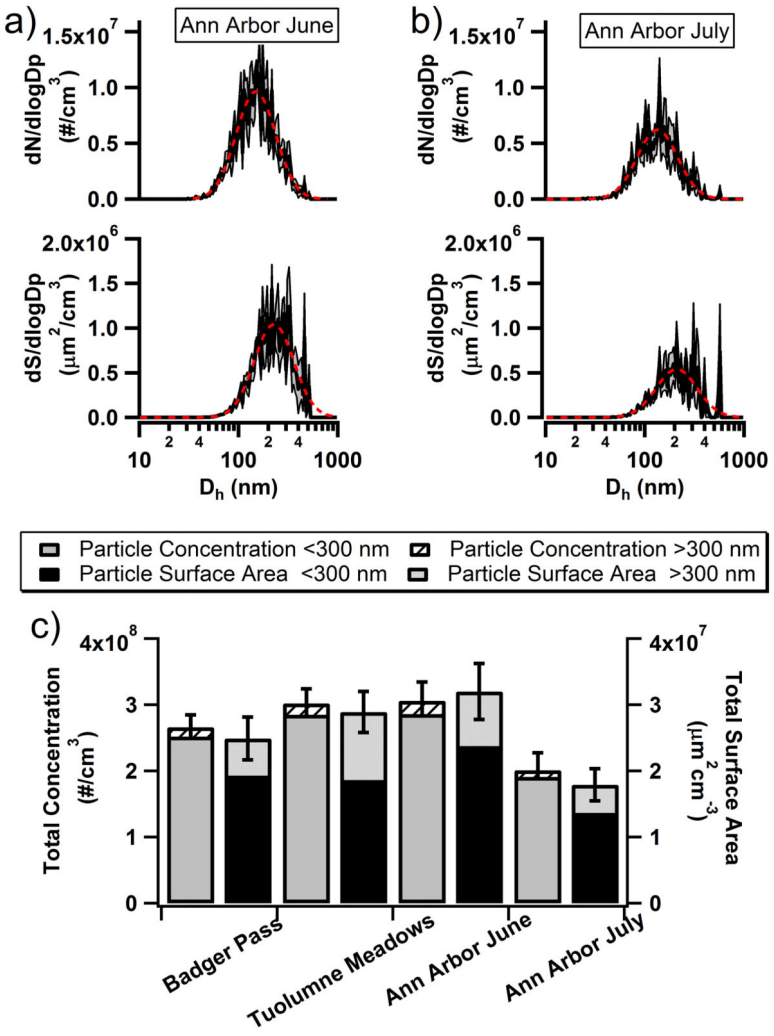

Figure 3.

Number size and surface area distributions for the Ann Arbor rain samples from a) June and b) July collected using the NTA. The dashed (red) lines are log-normal fits for the number size and surface area distributions and the (grey) shaded regions indicate the ± 1 standard error of the mean. c) The total number concentration and surface area of particles from all 4 precipitation samples is given with standard error and includes the fractional break down of large (>300 nm) and small (<300 nm) particles.

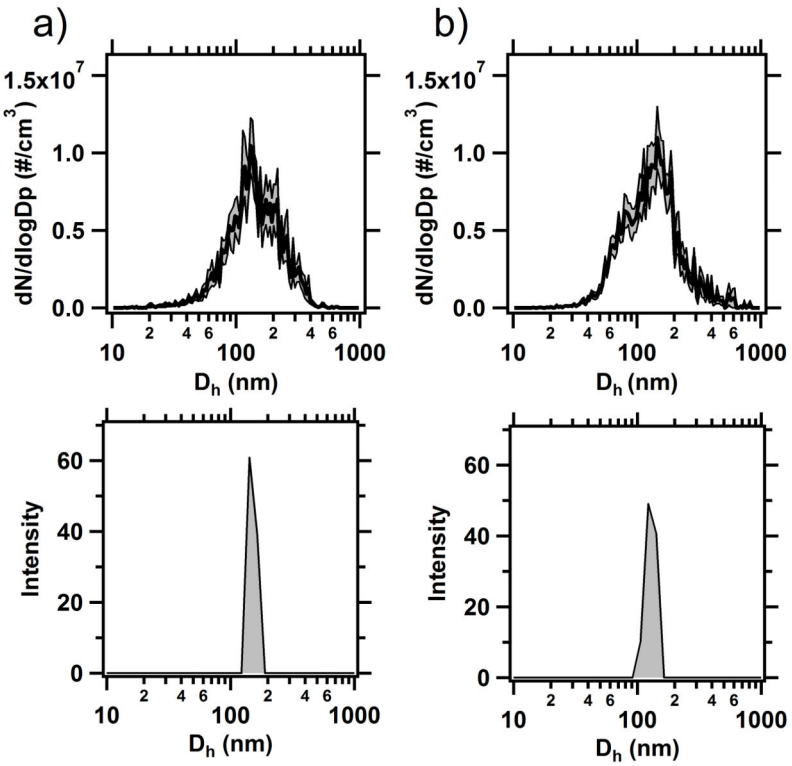

Figure 4.

Comparison of sizing data for snow samples collected from a) Badger Pass and b) Tuolumne Meadows using NTA and DLS. The (grey) shaded region on the NTA samples indicates the ± 1 standard error of the mean.

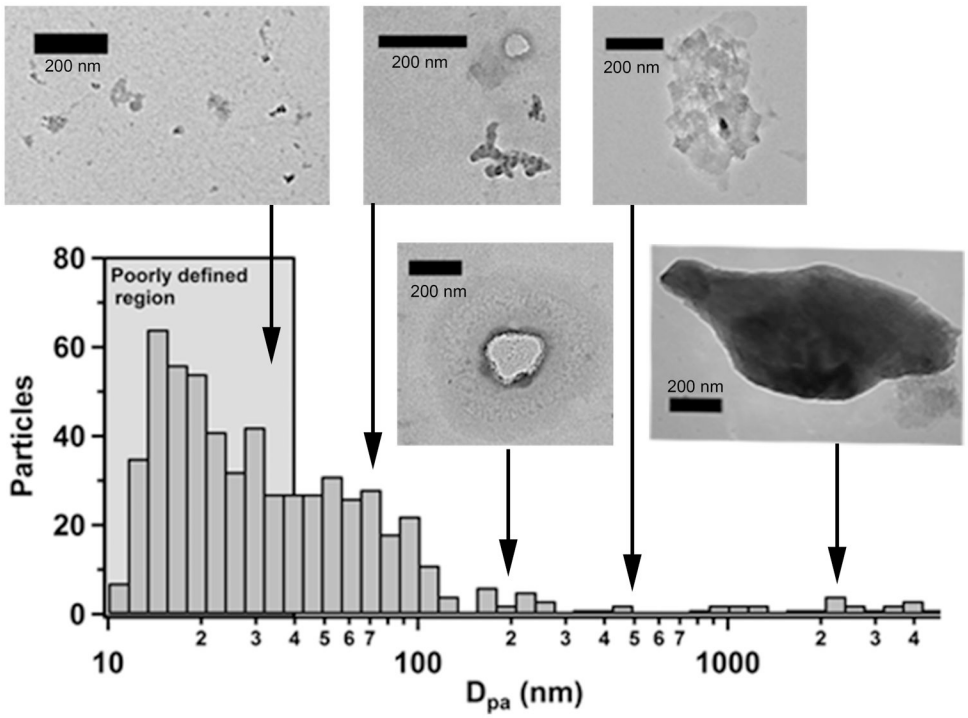

Figure 5.

Representative TEM size distribution and images of particles in the snow melt samples collected at Tuolumne Meadows. Only 3.4% of the particles were observed to be greater than 1 μm in size.

Table 1

The total concentration and log-normal fitted mode centers for number and surface area distributions collected using NTA identified for all four of the precipitation samples. Bolded numbers indicate the peak mode of the distribution.

Sample	Size Distribution	Modes (nm)	Total Concentration*
Badger Pass	Number	**133**, 261	$2.7(\pm0.2)\times10^{8}$
	Surface Area	148, **270**	$2.5(\pm0.8)\times10^{7}$
Tuolumne Meadows	Number	80, **148**, 227	$3.0(\pm0.2)\times10^{8}$
	Surface Area	**173**, 461	$2.9(\pm0.1)\times10^{7}$
Ann Arbor June	Number	150	$3.0(\pm0.3)\times10^{8}$
	Surface Area	228	$3.2(\pm1.0)\times10^{7}$
Ann Arbor July	Number	134	$2.0(\pm0.3)\times10^{8}$
	Surface Area	210	$1.8(\pm0.7)\times10^{7}$

*Total number concentration units are in particles cm^{-3} and for total surface area in μm^2 cm^{-3}.